Smart alloys as armor material for DEMO: overview of properties and joining to structural materials

Felix Klein[a], Andrey Litnovsky[a,b], Xiaoyue Tan[a,c], Jesus Gonzalez-Julian[a], Marcin Rasinski[a], Christian Linsmeier[a], Martin Bram[a], Jan Willem Coenen[a,d]

[a] *Forschungszentrum Jülich GmbH, Institut für Energie- und Klimaforschung, 52425 Jülich, Germany*
[b] *Department of Plasma Physics, Institute of Laser and Plasma Technologies National Research Nuclear University MEPhI, Kashirskoe sh., 31, 115409 Moscow, Russian Federation*
[c] *School of Materials Science and Engineering, Hefei University of Technology, Hefei, 23009, China*
[d] *Department of Engineering Physics, University of Wisconsin - Madison, Madison, WI 53706, USA*

Abstract

Tungsten test is currently the baseline first-wall armor material for a future DEMOnstration power plant. Smart alloys, containing tungsten (W), 11.4 weight – % chromium (Cr), and 0.6 weight – % yttrium (Y), aim at achieving passive safety in case of air ingress into the vacuum vessel and a loss-of-coolant accident causing a temperature rise above 1200 K for weeks. In such a case, smart alloys suppress oxidation and sublimation of radioactive W.

This publication summarizes several important properties of smart alloys: the suppression of oxidation, the hardness as a function of the microstructure, and potential carbide formation in the presence of carbon (C) impurities. Further, first results on joining them to the EUROFER by field-assisted sintering technology (FAST) without interface layer are presented. In literature, FAST is also known as spark plasma sintering (SPS). A stable joint with an tungsten-iron (W-Fe) diffusion layer of 100 nm at the interface was achieved. The joint survived several heat cycles to 873 K.

Keywords: Tungsten alloys, smart alloys, joining, DEMO, safety, oxidation, W-Cr-Y alloys, Sublimation

1. Introduction

Tungsten (W) is the current baseline material as first-wall armor material in future DEMOnstration power plants. Main advantages are its resistance to heat and particle loads, good thermal conductivity and low tritium retention. The fusion neutrons activate W, but the material is recyclable after 100 years [1]. The development of smart alloys addresses full passive safety in case of a loss-of-coolant accident (LOCA) in combination with air ingress into the vacuum vessel. The nuclear decay heat would cause a temperature rise to 1200 K for several weeks [2]. Under these conditions, in humid air at a temperature of 1273 K to 1450 K, the radioactive oxide will oxidize and sublimate at a rate of 1.4×10^{-4} mg cm^{-2} s^{-1} [3] causing a severe hazard to the environment.

Therefore, oxidation-resistant W alloys are developed to provide passive safety in case of the aforementioned accident. They are called 'smart alloys' as they automatically adapt their properties to the environment - featuring a W-like erosion resistance to the plasma, coupled with an outstanding oxidation resistance when required. Previous studies reported a similar erosion resistance of smart alloys as compared to that of pure W [4, 5]. Further, a superior oxidation resistance as compared to that of pure W was reported: at 1273 K the sublimation rate in humid air is suppressed by a factor of more than 40 [3] as compared to that of pure W. Here, this phenomenal progress is illustrated by photographs of pure W in Fig. 1 (a) and the smart alloy in Fig. 1 (b). Both samples were oxidized at 1273 K in synthetic air. W showed huge volume increase due to the formation of WO_3 while the smart alloy conserved its shape and formed a protective Cr_2O_3 layer on the surface. One corner of the sample shown in Fig. 1 (b) was cut in order to visualize the clean metal below the protective oxide. Nevertheless, it must be noted that the protective mechanisms work only up to 1273 K and fail at higher temperatures [3].

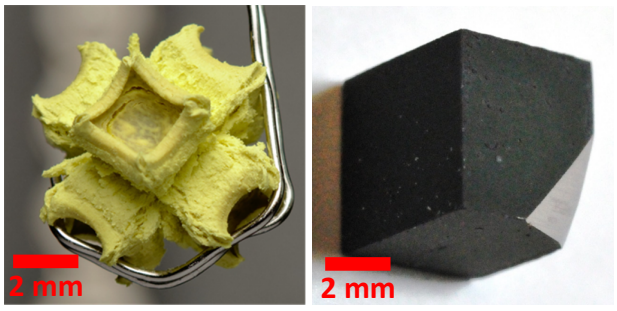

(a) Tungsten (b) Smart Alloy

Figure 1: Photographs of **(a)** W after only 10 h and **(b)** smart alloy after 2 days of oxidation at 1273 K. W shows massive volume expansion and no oxidation resistance while the smart alloy develops a protective oxide layer on top of the alloy which is visualized by the cut corner.

Email address: fe.klein@fz-juelich.de (Felix Klein)

In this paper three main topics are addressed: first, the microstructure and its influence on the hardness. Second, observations on carbide formation are shown and the consequences are discussed. Third, the possibility of joining smart alloys to EUROFER using field-assisted sintering technology without interlayer material is tested. The resulting joint is imaged and tested under thermal cycling conditions.

2. Experimental

Smart alloys are manufactured via a powder-metallurgial route. The elemental powders are mechanically alloyed in a planetary ball mill. The alloyed powder is sintered using field-assisted sintering technology (FAST). More details on the parameters and the optimization process are found in [5, 6, 7]. The elemental composition is 88 wt % W, 11.4 wt % Cr, and 0.6 wt % Y in the following written as W – 11.4Cr – 0.6Y. Specific parameters for the milling process and the FAST joining process are given in section 3 and 5, respectively.

Electron microscopy, including scanning transmission electron microscopy (TEM), is performed using the Crossbeam 540 manufactured by Carl Zeiss. Cross sections and TEM-lamellas are cut using a focussed ion beam. Elemental quantification is performed using energy-dispersive X-ray spectroscopy (EDX). The grain size is determined by counting the grains on a cross section in a rectangular area and normalizing the result to the number of grains per μm^2.

Chemical analysis on carbon (C) impurities is performed using the LECO CS600 device. Calibration is performed using reference materials provided by LECO.

The density is measured using Archimedes principle. A relative density of >97 % is measured for all smart alloys presented in this work.

The Vickers hardness (HV0.5) is measured by micro-indentation. Using a diamond-tip an indent into the material is created and measured optically. Typically the indent has a diagonal of around 27 µm. 10 indentations are preformed on each material, then the average is calculated.

Thermal cycling is performed using the device TAG 16/18 manufactured by Setaram. Details on the thermal cycling test are given in section 5.

3. Microstructure

The influence of the microstructure on oxidation was published already in [6]. In this paper a complementary study on the hardness is presented. In [6] it was found that a grain size of around 36 grains/μm^2 is required for acceptable oxidation resistance. At that time, this was the smallest achieved grain size. Now, a new mill ('PM400 MA' manufactured by Retsch) is available. Previously, we used the 'PM400' manufactured by Retsch. The difference is a higher rotation ratio of 1:-3 of the jars and the planetary wheel in the PM400 MA as compared to the rotation ratio of 1:-2 in the PM400. The new mill allows achieving finer grain sizes down to 127 grains/μm^2. Dedicated studies on a comprehensive overview on the effects of changing the mill are ongoing and will be published elsewhere.

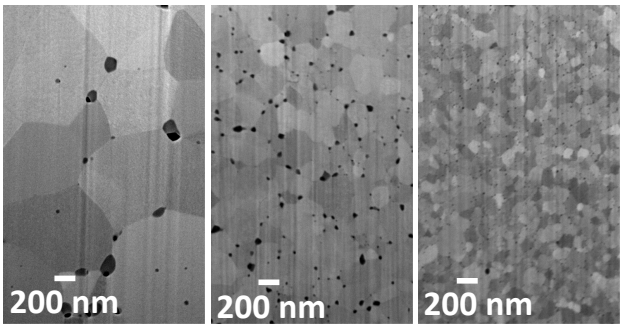

(a) (b) (c)

Figure 2: Exemplary W – 11.4Cr – 0.6Y alloys with different microstructures were sintered. **(a)** features 2 grains/μm^2, **(b)** features 19 grains/μm^2, and **(c)** features 127 grains/μm^2

Fig. 2 shows the microstructure of three exemplary W – 11.4Cr – 0.6Y alloys:

- Fig. 2 (a) shows an alloy with 2 grains/μm^2. The powder was alloyed using the PM400 device. During sintering a heating rate of 100 K/min to the maximum temperature of 1733 K and a holding time of 1 min at that temperature were used. As compared to the other samples the heating rate is low and there is a holding time at the maximum temperature. Both parameters yield grain growth in the material.

- Fig. 2 (b) shows an alloy with 19 grains/μm^2. The powder was alloyed using the PM400 device. During sintering an increased heating rate of 200 K/min to the maximum temperature of 1733 K and no dwell time were used.

- Fig. 2 (c) shows an alloy with 127 grains/μm^2. The powder was alloyed using the PM400 MA device. The same sintering parameters as in (b) were used. Dedicated studies on the mechanisms yielding the smaller grain size are ongoing.

The influence of the grain size on hardness is shown in Fig. 3. Within the investigated range from 2 grains/μm^2 to 127 grains/μm^2, the hardness decreases with increasing grain size. This observation is well known as grain-boundary strengthening / Hall-Petch relationship. A very high hardness is problematic as hard materials are prone to cracking. During electrical

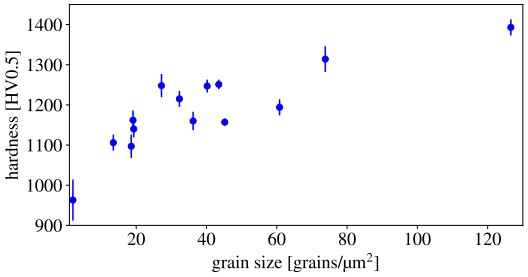

Figure 3: The hardness of W – 11.4Cr – 0.6Y alloys is shown as a function of grain size. Each data point is measured on a different sample.

discharge machining around 25 % of the samples with a Vickers hardness $HV0.5 > 1250$ cracked, while no sample with a hardness $HV0.5 < 1150$ broke.

Therefore, the optimum grain size seems to be around 20 grains/µm^2 to 30 grains/µm^2, corresponding to a grain diameter of around 0.2 µm, as the oxidation resistance remains good and cracking during machining is avoided. It must be noted that this grain diameter has no physical significance as it represents the side of a square grain. However, the cross sections show that the grains are not squares.

4. Carbides

The jar and the milling balls used during mechanical alloying are made from tungsten carbide (WC) with cobalt (Co) binder. The mechanical alloying is essential in order to achieve a homogeneous, solid solution of the alloy. WC offers multiple advantages: it has a high density resulting in a high impact energy onto the powder particles, which is important for efficient alloying. It has a high hardness resulting in little wear during alloying. Further, one potential main impurity is W, which is the main component of the alloy anyways. The Co concentration seems to scale with the C impurities at an atomic concentration ratio C/Co = 7 as expected from ~ 5 wt % Co binder in the WC tools and measured by atom probe tomography on one sample. Thus, the Co concentration is in the 10^{-3} wt % range and its influence on the alloy is not analyzed independently of C in this work. C is a potential main impurity. Depending on the milling parameters 5×10^{-3} wt % to 150×10^{-3} wt % of C are measured in the alloy.

From steels it is known that chromium carbides often form at the grain boundaries [8, 9]. Such a precipitation of carbides can have a significant impact on subsequent precipitation of alloying elements within the component [10, 9]. The Gibbs free energy for the formation of chromium carbide ($Cr_{23}C_6$) with −78 kJ/(mol C) is about twice as negative as the one of WC with −35 kJ/(mol C). Thus, energetically it is favorable to form $Cr_{23}C_6$ over WC. For the composition of the present alloy, the W-Cr-C phase diagram [11, 12] predicts full solid solution at ~1600 K which is exceeded during sintering. However, already starting below ~1500 K, C can no longer be dissolved [11, 12]. Thus, C is expected to accumulate at the grain boundaries and potentially form $Cr_{23}C_6$. When sintering W − 10Cr − 1Hf at around 2000 K dealloying via mechanisms of liquid phase sintering were observed in the presensce of carbon foil [13]. The usage of W foil as a C barrier is discussed [13]. In this work, the maximum sintering temperature is only 1733 K reducing the diffusion of carbon from the foil as compared to the aforementioned work.

An alloy containing 5×10^{-2} wt % C was selected for fundamental TEM investigations. After sintering the sample was heated at 1073 K for one hour. The results are shown in Fig. 4. Fig. 4 (a) shows an overview image. The darker grains have an increased Cr content and can be assigned as Cr-rich phase while the brigher grains have a lower Cr content and can be assigned as Cr-poor phase. In addition, Y-enriched nano particles are

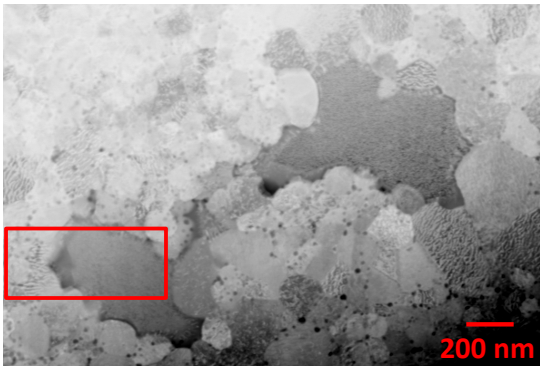

(a)

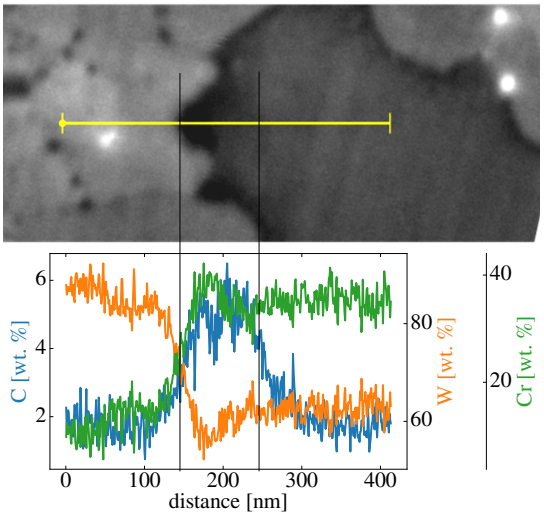

(b)

Figure 4: Scanning transmission electron microscopy of W − 11.4Cr − 0.6Y with 5×10^{-2} wt % C after heat treatment at 1073 K for 1 h. **(a)** shows an overview image, the red box indicates the region of image (b). **(b)** includes an energy dispersive x-ray line scan at an electron energy of 5 keV.

visible at the grain boundaries. Close examination of the image suggests that the Cr-rich phase is encapsulated by a fourth phase.

Fig. 4 (b) shows a zoom to the rectangular red box including an EDX line scan across the interface of the Cr-rich and Cr-poor phase. There are three signals plotted for the EDX line scan: the W signal is around 87 wt % in the Cr-poor phase and reduced to around 63 wt % in the Cr-rich phase. On the contrary, the Cr signal is around 10 wt % in the Cr-poor phase and as increased to around 35 wt % in the Cr-rich phase, as to be expected. The C signal is influenced by the W signal as the C signal is determined using the peak at 0.277 keV while W has an overlapping transition at 0.25 keV. Therefore, the absolute numbers on the C concentration in the plot cannot be trusted. Nevertheless, the C signal exhibits a peak at the interlayer despite that the W signal has already dropped by one forth. These observations allow the conclusion that Cr-C, potentially also containing W, has formed at the interface of the Cr-rich and Cr-poor phase.

In conclusion, the expectation from literature that C may form Cr-C at the grain boundaries is confirmed. Such a carbide formation may impact the material properties adversely,

for instance increase the brittleness or degrade the oxidation resistance. Dedicated studies on the effects are still ongoing - but the authors assume already that the C contamination of smart alloys must be minimized. Currently, it seems that the level of $\sim 5 \times 10^{-3}$ wt % achieved in the sample shown in Fig. 2 b and analyzed in [3] is sufficient. Nevertheless, this knowledge is important for up-scaling of the production and investigation of the effects of further reduction of the C content are interesting. Possible attempts for reduction of the C content are the further optimization of the mechanical alloying parameters or changing the mechanical alloying tools. Candidates for the substitution of WC are yttrium stabilized zirconia or steel, which will result in other impurities that must be studied.

5. Joining

Joining the first wall armor material to the structural steel is an important challenge on the way to realization of the first wall of DEMO. There are various approaches to join W: brazing [14], functionally graded materials [15], or hot isostatic pressing [16]. In any case, the aim is to achieve a stable joint that can withstand the thermal stresses occurring due to a different thermal expansion coefficients. Currently, it is not known how smart alloys behave during joining and whether the technologies applied on W are applicable for smart alloys.

Here, first results of the attempt to join smart alloys and EUROFER directly using the FAST technique are shown. No interlayer material between EUROFER and the smart alloy was used, the surface of both the EUROFER and the smart alloy with the size of 1 cm by 1 cm were polished to mirror-finish with active oxide polishing suspension before joining. The test was performed at a pressure of 50 MPa in vacuum (5 mbar) and a heating rate of 200 K/min to the maximum temperature of 1073 K. At this temperature and a pressure of 50 MPa the sample was held for 1 h. Then, the sample was cooled at 200 K/min without further treatment.

Afterwards, the joint was cut and ground in preparation for TEM imaging. The joint appeared sufficiently strong to withstand all machining steps. The results of the TEM study are shown in Fig. 5. The electron image shows an overview. At the interface there are pores on the nm-size as labeled. Further, there appears a diffusion layer with a thickness of around 0.1 µm at the interface. An EDX line scan across the interface is performed in order to determine its composition, the result is also shown in Fig. 5. The interface appears to contain mainly W and Fe.

In a first test the behavior of the joint under mild thermal cycling is determined. Seven cycles were performed between 573 K and 873 K. The holding time was 2 h at the higher temperature and 0.5 h at the lower temperature. Theses times are according to the pulse duration estimates for DEMO by C. Harrington [17] where a flat-top pulse with a duration of 2 h and a dwell period of 0.5 h are assumed. Harrington [17] states a that the linear ramping of the power between the two states takes 300 s, which would correspond to a heating rate of 60 K/min. Unfortunately, such a heating rate cannot be achieved using the available equipment and a lower heating rate of 10 K/min was used.

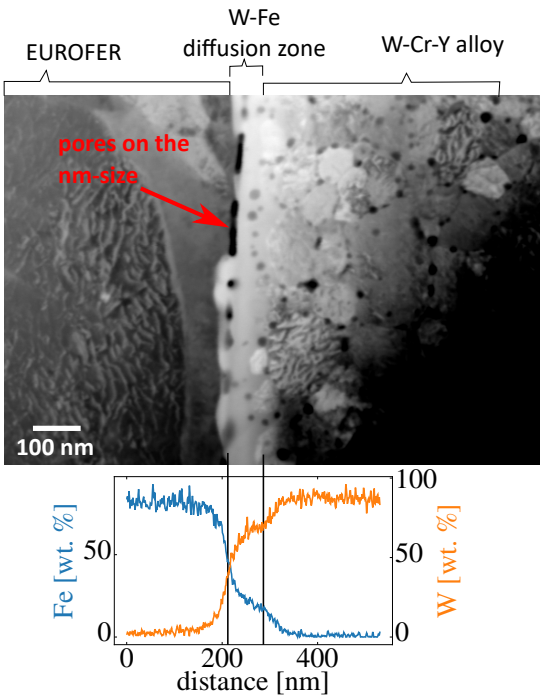

Figure 5: Joint between EUROFER and smart alloy. The top part shows an transmission electron microscopy image visualizing the diffusion zone at interface and pores on the nm-size. The energy dispersive x-ray line scan across the interface confirms an W-Fe diffusion zone at the interface.

No macroscopic changes were observed after the thermal cycling experiment. A cross section is shown in Fig. 6. Please note, this is a standard cross section, not imaging of a TEM lamella. Therefore, the diffusion zone cannot be visualized, neither in the electron image nor in an EDX scan. However, the main purpose of this work is to study if the joint remained intact after thermal cycling. And indeed, no indications for a macroscopic failure of the interface were detected.

In conclusion, the preliminary results are promising and the employed joining technology should be further investigated and optimized. For instance, the properties of EUROFER may change during the joining at 1073 K, Zilnyk [18] reports that major changes in the microstructure occur in the first hour of annealing at 1073 K. Therefore, it remains to be tested whether the temperature during joining can be reduced further or whether the holding time can be reduced. The authors are optimistic that optimizations are possible. Further, it will be important to see how the joint behaves under more realistic thermal cycling with more stresses due to higher heating rates and steeper temperature gradients.

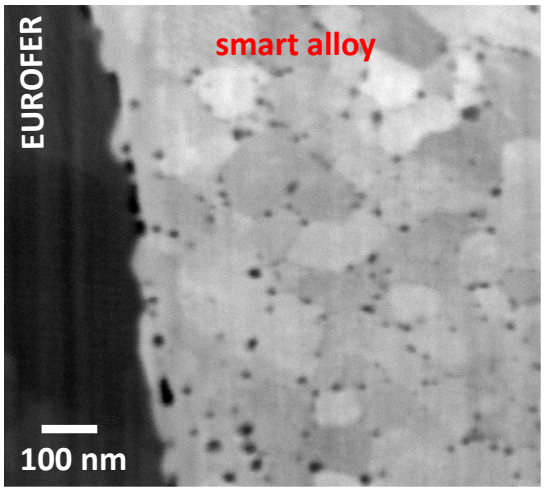

Figure 6: Scanning electron microscopy on a cross section, not on a lamella, after 7 thermal cycles from 573 K to 873 K with a holding time of 0.5 h and 2 h, respectively.

6. Conclusions

Smart alloys, containing W – 11.4Cr – 0.6Y, as first wall armor material may offer intrinsic safety for future fusion power plants in case of a loss-of-coolant accident including air ingress into the vacuum vessel. The oxidation is suppressed successfully at up to 1273 K and the sublimation is suppressed $40x$ in humid air.

The grain size of the alloy must be controlled. The microstructure, thus also the grain size, is influenced by the sintering process, but also by the mechanical alloying process and the carbon content. It is shown that a decreased grain size down to around 130 grains/μm^2 increases the hardness of the material, creating difficulties with machine-ability. However, previous publications showed that an increased grain size of around 2 grains/μm^2 degrades the oxidation resistance [6]. Therefore, the optimum grain size is around 20 grains/μm^2 to 30 grains/μm^2.

Further, it is shown that C concentrations as low as 5×10^{-2} wt % influence the microstructure. Chromium carbides were detected by TEM after heat treatment. The hypothesis is that these carbides degrade the properties of the alloy, in particular its brittleness and oxidation resistance. A dedicated study on the influence of carbon on smart alloys will be published elsewhere.

Further, in this work it is shown that EUROFER and smart alloy can be joined successfully using FAST without interlayer material. Despite pores of a nm-size being detected at the interface, a W-Fe diffusion layer holds the joint tightly and no failure is observed after 7 thermal cycles between 573 K and 873 K with a holding time of 0.5 h and 2 h, respectively. Therefore, this joining method seems promising and in a next step optimization and real thermal cycling with realistic temperature gradients and higher heating rates should be performed.

7. Outlook

Generally, the proof of principle - oxidation resistance [3] and plasma resistance [5] of smart alloys is achieved. Future work must solve the technological challenges on how to apply smart alloys. This task requires a solid scientific understanding of the material. Such an understanding includes the mechanisms of neutron degradation and acquisition of the phase diagram including the role of impurities.

Aforementioned knowledge will allow predictions on the aging and possible degradation of the alloy and the interface to EUROFER. Further, it will allow to define impurity tolerances for industrial production of the alloyed powder. Mechanical alloying using steel tools would result in a significant cost reduction but also in the introduction of a few percent of iron. Therefore, the tolerances must not be limited to C and iron is also of interest. Realistic cost estimations for a DEMO first wall with smart alloys can be made once this knowledge is available.

Acknowledgements

A part of this work has been carried out within the framework of the EUROfusion Consortium and has received funding from the Euratom research and training programme 2014 - 2018 and 2019 - 2020 under grant agreement No 633053. The views and opinions expressed herein do not necessarily reflect those of the European Commission.

References

[1] M. R. Gilbert, J.-C. Sublet, and R. A. Forrest. *Handbook of activation, transmutation, and radiation damage properties of the elements simulated using FISPACT-II & TENDL*. Culham Center For Fusion Energy, 2015.

[2] D. Maisonnier, I. Cook, P. Sardain, L. Boccaccini, E. Bogusch, K. Broden, L. Di Pace, R. Forrest, L. Giancarli, S. Hermsmeyer, et al. The european power plant conceptual study. *Fusion Eng. Des.*, 75:1173–1179, 2005.

[3] F. Klein, A. Litnovsky, T. Wegener, X. Y. Tan, J. Gonzalez-Julian, M. Rasinski, J. Schmitz, Ch. Linsmeier, M. Bram, and J. W. Coenen. Sublimation of advanced tungsten alloys under DEMO relevant accidental conditions. *Fusion Eng. Des.*, 146(A):1198–1202, 2019.

[4] J. Schmitz. *Development of tungsten alloy plasma-facing materials for the fusion power plant*. doctoralthesis, Ruhr-Universität Bochum, Universitätsbibliothek, 2020.

[5] A. Litnovsky, J. Schmitz, F. Klein, K. De Lannoye, S. Weckauf, A. Kreter, M. Rasinski, J. W. Coenen, Ch. Linsmeier, J. Gonzalez-Julian, et al. Smart tungsten-based alloys for a first wall of demo. *Fusion Eng. Des.*, 159:111742, 2020.

[6] F. Klein, T. Wegener, A. Litnovsky, M. Rasinski, X. Y. Tan, J. Gonzalez-Julian, J. Schmitz, M. Bram, J. W. Coenen, and Ch. Linsmeier. Oxidation resistance of bulk plasma-facing tungsten alloys. *Nucl. Mater. Energy*, 15:226–231, 2018.

[7] F. Klein, M. R Gilbert, A Litnovsky, J. Gonzalez-Julian, S. Weckauf, T. Wegener, J. Schmitz, Ch. Linsmeier, M. Bram, and J. W. Coenen. Tungsten-chromium-yttrium alloys as first wall armor material: Yttrium concentration, oxygen content and transmutation elements. *Fusion Eng. Des.*, 158:111667, 2020.

[8] M. F. McGuire. *Stainless Steels for design engineers, Chapter 4: Corrosion Types, p. 27-56*. ASM International, 2008.

[9] K.H. J. Buschow, editor. *Encyclopedia of Materials: Science and Technology*. Elsevier Ltd., 2001.

[10] P. L. Andresen. *Stress corrosion cracking (SCC) of austenitic stainless steels in high temperature light water reactor (LWR) environments*. Number p. 236-307. Woodhead Publishing Series, 2010.

[11] P. Villars. C-Cr-W isothermal section of ternary phase diagram, 2020.

[12] P. Stecher, F. Benesovsky, and H. Nowotny. Untersuchungen im System Chrom-Wolfram-Kohlenstoff. *Planseeberichte für Pulvermetallurgie*, 12:89–95, 1964.
[13] M. Vilémová, F. Lukác, J. Veverka, K. Illková, and J. Matejicek. Controlling the carbide formation and chromium depletion in W-Cr alloy during field assisted sintering. *International Journal of Refractory Metals and Hard Materials*, 79:217–223, 2019.
[14] D. Bachurina, A. Suchkov, A. Filimonov, I. Fedotov, M. Savelyev, O. Sevryukov, and B. Kalin. High-temperature brazing of tungsten with steel by cu-based ribbon brazing alloys for demo. *Fusion Eng. Des.*, 146(A):1343–1346, 2019.
[15] S. Heuer, B. S. Li, D. E. J. Armstrong, Y. Zayachuk, and Ch. Linsmeier. Microstructural and micromechanical assessment of aged ultra-fast sintered functionally graded iron/tungsten composites. *Mater. Des.*, 191, 2020.
[16] J. Y. Park, Y. I. Jung, B. K. Choi, D. W. Lee, and S. Cho. Joining of tungsten to ferritic/martensitic steels by hot isostatic pressing. *J. Nucl. Mater.*, 442(1-3):S541–S545, 2013.
[17] C. Harrington. Dynamic modelling of balance of plant systems for a pulsed DEMO power plant. *Fusion Eng. Des.*, 98-99:2147–2151, 2015.
[18] K. D. Zilnyk, H. R. Z. Sandim, R. E. Bolmaro, R. Lindau, A. Möslang, A. Kostka, and D. Raabe. Long - term microstructural stability of oxide-dispersion strengthened eurofer steel annealed at 800c. *J. Nucl. Mater.*, 448(1-3):33–42, 2014.

Highlights

- Joining smart alloys to EUROFER without interface layer was achieved by FAST.
- W-Fe diffusion zone formed at the interface during joining.
- Hardness decrease with increasing grain size was shown experimentally.
- Chromium-carbides were detected around Cr-rich phases using STEM.